Laboratory measurements of water vapour continuum absorption in spectral region 5000-5600 cm^{-1}: Evidence for water dimers

By IGOR V. PTASHNIK[1, 3]*, KEVIN M. SMITH[2], KEITH P. SHINE[1] and DAVID A. NEWNHAM[2, 4]

[1] *Department of Meteorology, University of Reading, UK*
[2] *Space Science and Technology Department, Rutherford Appleton Laboratory, UK*
[3] *Current affiliation: Institute of Atmospheric Optics, Russia*
[4] *Current affiliation: TeraView Ltd, UK*

Revised 27 May 2004

SUMMARY

In spite of decades of extensive studies, the role of water dimers (WD) in the atmospheric radiation budget is still controversial. In order to search for evidence of the dimer in the solar near infrared, high spectral resolution pure water vapour absorption spectra were obtained in laboratory conditions for two different pressures and temperatures in the spectral region 5000-5600 cm^{-1} (1.785 to 2 μm). The residual was derived as a difference between the measured optical depth and the calculated one for water monomer using the modified HITRAN database and two different representations of the water vapour continuum: CKD-2.4 (Clough-Kneizys-Davies) and the Ma and Tipping continuum. In both cases the residuals obtained are very similar to those expected from a recent theoretical calculation of the WD absorption. However, the WD band halfwidth at half maximum (HWHM) and dimerization equilibrium constant $K_{eq}(T)$, required to provide a best fit to the residual, differ for each case. To be in best agreement with the residual calculated by using the Ma and Tipping continuum, the WD bands HWHM should be ~28 cm^{-1}, and $K_{eq}= 0.02\pm0.0035$ atm^{-1} and 0.043 ± 0.0055 atm^{-1} for the temperatures 342 K and 299 K respectively. For the residual calculated using the CKD-2.4 continuum the fitted value of the HWHM is ~18 cm^{-1}, and $K_{eq}= 0.011\pm0.0025$ atm^{-1} (342 K) and 0.018 ± 0.003 atm^{-1} (299 K). It is concluded that a substantial part of the WD absorption is already implicitly included within the CKD-2.4 continuum model. The increase in estimated clear-sky global mean absorption of solar radiation due to water dimer varies from 0.5% to 2.0%, depending on the set of WD parameters used. On the basis of a comparison of the derived K_{eq} values with others in the literature, the higher estimate is favoured.

KEYWORDS: Dimerization equilibrium constant, CKD continuum, Ma and Tipping continuum, Radiative transfer

1. INTRODUCTION

Water vapour is one of the most important substances in the atmosphere. The absorption of solar radiation in the near infrared and visible spectral region is dominated by H_2O molecular absorption. In addition to the water monomer (WM), water clusters, such as water dimers (WD) or trimers, have been investigated very intensively in recent years (Mhin *et al.* 1993; Huisken *et al.* 1996; Low and Kjaergaard 1999; Vaida and Headrick 2000; Evans and Vaida 2000). In particular, the role of the water dimer in the atmosphere is still controversial, in spite of many theoretical and experimental investigations. An overview can be found, for example, in Vaida *et al.* (2001).

There are two interrelated issues in estimating the role of WD in the radiation budget. Firstly, it is necessary to know the parameters (intensity, width, position and shape) of the WD absorption bands. Secondly, it is important to know the abundance of the dimers. There is significant uncertainty in both these aspects.

Water dimers have recently been investigated (Arking 1999; Chylek *et al.* 1999; Daniel *et al.* 1999; Hill and Jones 2000; Vaida *et al.* 2001; Goldman *et al.* 2001) as a possible reason for the discrepancy between atmospheric absorption measurements and model calculations (Ramanathan and Vogelmann 1997; Kato *et al.* 1997, Conant *et al.* 1998, Arking 1999, Pilewskie *et al.* 2000). The upper limit of solar radiation absorption by WD varies between different authors from 1.5 to 6 Wm^{-2} for clear-sky tropical atmosphere and overhead sun (Daniel *et al.* 1999; Chylek *et al.* 1999; Vaida *et al.* 2001; Kjaergaard *et al.* 2003). According to the Goldman *et al.* (2001) calculation of water dimerization equilibrium constant K_{eq}, that defines WD amount for a given WM amount, the value of WD radiative absorption could be even 2-3 times higher.

Finally, water dimer has also been discussed as a possible component of the self-broadening part of water vapour continuum (Penner and Varanasi 1967, Devir *et al.* 1994). The similarity in the self-broadened continuum absorption and the calculated one due to WD can be seen in the Fig. 1; here the optical depth of water continuum model (Clough-Kneizys-Davies) CKD-2.4 (Mlawer *et al.* 1999) as well as the total WM absorbance is presented together with WD's optical depth for the spectral region 1000-15000 cm^{-1}. The latest calculations of Schofield and Kjaergaard (2003) of WD fundamental and overtone OH-stretching and HOH-bending vibrational transition frequencies and intensities were used to simulate the WD absorption. The water dimer band half-width at half-maximum (HWHM) was chosen to be 25 cm^{-1} for all WD bands together with an assumption that the wings are Lorentzian. The Curtiss *et al.* (1979) WD's enthalpy and entropy parameters (ΔH= -3.59 kcal mol^{-1}, ΔS= -18.59 cal $K^{-1}mol^{-1}$) were used to calculate K_{eq}:

$$K_{eq} = \exp(\Delta S/R - \Delta H/RT), \quad (1)$$

where R is the universal gas constant and T is temperature. It is worth mentioning that the temperature dependence $K_{eq}(T)$ is very similar to that for water CKD continuum. Moreover, the self-broadened water vapour continuum has the same quadratic dependence on WM partial pressure p_{WM} as the WD:

$$p_{WD} = K_{eq} \cdot p_{WM}^2. \quad (2)$$

This causes a very similar relation between WD and CKD continuum absorption (to that presented in the Fig. 1) for the other pressures and temperatures.

Theoretical and experimental investigations of WD's thermodynamic and chemical properties can be found in Curtiss *et al.* (1979), Slanina and Crifo (1992), Mhin *et al.* (1993), Munoz-Caro and Nino (1997), Headrick and Vaida (2001) and Goldman *et al.* (2001). The different approaches to derive WD spectroscopic parameters were described by Huang and Miller (1989), Huisken *et al.* (1996), Tso *et al.* (1998), Low and Kjaergaard (1999), Perchard (2001), Schofield and Kjaergaard (2003), and by many other authors.

In spite of this interest in water dimers, two attempts to detect direct WD absorption in the atmosphere have failed (Daniel *et al.* 1999; Hill and Jones 2000). There are two main reasons why it is so difficult to detect WD in the atmosphere. First, WD absorption is usually masked by strong WM absorption (see Fig. 1). Second, there is a big uncertainty in knowledge of the main WD parameters. For example, estimates of the dimerization equilibrium constant K_{eq} vary from ~0.01 atm^{-1} (Mhin *et al.* 1993) to ~0.12 atm^{-1} (Goldman *et al.* 2001) for room temperature. The theoretically predicted and observed WD fundamental and overtone band's HWHM can vary from 6 cm^{-1} to 100 cm^{-1} (Vaida *et al.* 2001). The ab-initio calculated WD cross-section spectrum has also changed markedly during recent years (Tso *et al.* 1998; Low and Kjaergaard 1999;

Schofield and Kjaergaard 2003). Such an uncertainty makes it very difficult to predict the best spectral region to detect WD dimers. For example, the two experimental attempts mentioned above filed to reproduce the calculations of Tso *et al.* (1998) in the spectral region 10600-15000 cm^{-1} (0.66-0.94 μm). Vaida *et al.* (2001) attribute this mostly to the lack of a suitable dipole moment function in the Tso *et al.* (1998) model.

The only work to date that describes the detection of WD absorption in the atmosphere (the $|0\rangle_f|4\rangle_b$ overtone transition) in the spectral region near 13330 cm^{-1} (0.75 μm) has recently appeared (Pfeilsticker *et al.* 2003). Apart from this work, no other measurements (either laboratory or atmospheric) of WD absorption in equilibrium, close to atmospheric conditions, have been reported. The technique of creation of supersonic molecular beams is usually used to investigate WD properties (Huang and Miller 1989; Huisken *et al.* 1996; Paul *et al.* 1997), which, however, does not allow making any definite conclusion about possible WD amounts in atmosphere.

In the present work we will discuss the results of measurements and numerical simulation aimed at the direct detection of WD absorption in the spectral region 5000-5600 cm^{-1} (1.785-2.0 μm) in pure water vapour cell in laboratory condition. In spite of relatively strong overlapping with the WM absorption, there is predicted to be a significant absolute value of WD absorption in this region[1]. The measurement in a WM absorption band could help also to investigate the possible relation between WD and present models of water vapour continuum absorption.

2. EXPERIMENTAL SETUP

The near-infrared absorption spectra of pure water vapour for conditions presented in Table 1 have been characterised at the Rutherford Appleton Laboratory (RAL) Molecular Spectroscopy Facility using a combination of high resolution Fourier transform spectroscopy with fixed and variable path-length absorption cells. Measurements made at a path length of 29 cm have been described in detail previously (Smith *et al.* 2004). Here we report two additional measurements made using two variable path-length absorption cells. The long path-length absorption cell (LPAC), described previously (Ballard *et al.* 1994), is capable of providing optical path-lengths in the range 32 m to 1 km at temperatures between 200 K and 300 K. A short path-length cell (SPAC) (Remedios 1990) gives optical paths in the range 5 m to 20 m and temperatures in the range 200 K to 350 K. For this work the Bruker IFS 120HR Fourier transform spectrometer (FTS) was configured with a 150 W quartz tungsten halogen source, a calcium fluoride beam-splitter, and a liquid nitrogen-cooled indium antimonide (InSb) detector. The LPAC and SPAC fitted with calcium fluoride windows and gold-coated reflective optics was used.

TABLE 1. MEASUREMENT CONDITIONS

	H_2O pressure, hPa	Temperature, K	Path length, m	Resolution*, cm^{-1}	
1	98	342	9.74	0.03	(SPAC)
2	20	299	128	0.0068	(LPAC)
3	20	297	0.29	0.0068	

* Spectral resolution is defined here as 0.9/(maximum optical path difference in cm)

[1] Part of the reason for choosing the 5000-5600 cm^{-1} region was that the theoretical WD spectrum in Vaida *et al.* 2001 (H.G. Kjaergaard, personal communication) indicated more intense and distinct WD absorption in this spectral region (Fig. 1), than the recent more precise calculation (with a better representation of HOH-bending modes) by the same group (Schofield and Kjaergaard 2003), which was reported after our measurements.

The optical path length in the LPAC was 128 m at 299 K (see Table 1). The SPAC was operated at an optical path of 9.74 m and electrically heated to 342 K. Good stability of the water vapour partial pressure was achieved by virtue of the small surface-area-to-volume ratio of both the cells. Norton-Beer strong apodisation (Norton and Beer 1976) and Mertz phase correction (Mertz 1967) were applied to all of the measured interferograms. Where appropriate, optical filters were used to limit the optical bandwidth to the spectral range of the measurement. The interferometer input aperture diameter was set such that the intensity of radiation at the detector was sufficient to give excellent information-to-noise ratios, whilst avoiding saturation of the detector or loss of spectral resolution. The alignment of the interferometer was optimised and the photometric accuracy tested before carrying out the measurements reported here. The FTS was maintained at a pressure below 0.4 Pa by a turbo-molecular pump to minimise the amount of carbon dioxide and water vapour in the optical path of the interferometer. A calcium fluoride window separated the FTS from the SPAC transfer optics. A rotary and turbo-molecular pump evacuated the transfer optics to a pressure below 0.02 Pa.

Details of the sensors used to measure gas temperature, pressure, and humidity within the LPAC and SPAC are given in Table 2. The 10 Torr and 1000 Torr full-scale Baratron gauges (calibration traceable to NIST) were used to monitor pressure during sample preparation and throughout the measurements. The atmospheric pressure reading of the 1000 Torr Baratron was compared with that of a calibrated (traceable to UK National Physical Laboratory standards) precision aneroid barometer. Low-pressure readings of the 10 Torr and 1000 Torr Baratron gauges were compared by measuring identical pressures with both gauges. Relative humidity (RH) was measured with two humidity/platinum resistance thermometer sensors positioned at opposite ends inside either the LPAC or SPAC.

TABLE 2. DETAILS OF TEMPERATURE, PRESSURE AND HUMIDITY SENSORS

Measurement	Manufacturer and type	Stated uncertainty
Temperature:		
LPAC	Heraeus/Nulectrohms Platinum resistance thermometers (14 positions)	± 0.1 K at 273 K
SPAC	RS Components R-T curve matched negative temperature coefficient thermistors type UUA41J1 (6 positions)	±0.2 K at 296 K
Signal logger	Laplace Instruments Model SPC-801	±0.3 K
Pressure:		
0-10 hPa	MKS-390 (10 Torr Baratron)	±0.08% of reading
10-1000 hPa	MKS-390 (1000 Torr Baratron)	±0.08% of reading
Atmospheric	Negretti aneroid barometer M2236A	±40 Pa
Humidity:		
Relative humidity (RH) 0-90% / 90-100%	Vaisala HMP234	±1% / ±2%
Temperature	Vaisala HMP234	±0.1 K

Water vapour samples were prepared using a clean glass/PTFE vacuum line from distilled liquid water (analar grade, BDH Chemicals), which had previously been purified to remove dissolved air using at least three repeat 200 K freeze-pump-thaw cycles. Agreement between the humidity sensor and pressure gauge readings (to within the humidity sensor accuracy) confirmed the purity of the water vapour introduced to

the gas cells. The vapour pressure, RH and temperature were recorded at 5-second intervals during spectroscopic measurements on water vapour samples.

Evacuated-cell background spectra were recorded before and after each filling of the LPAC or SPAC, at a spectral resolution of 0.03 cm^{-1}. Before each background spectrum was recorded, high-resolution test measurements were made to check that the water vapour had been adequately removed from the gas cell. Taking the ratio of the sample and averaged background spectra minimised errors in the transmittance or absorbance spectra arising from changes in baseline signal level, e.g. due to drifts in the near-IR source intensity.

The measured water vapour transmittance $\tau(\tilde{\nu},T)$ at wavenumber $\tilde{\nu}$ and temperature T was calculated using $\tau(\tilde{\nu},T)=I(\tilde{\nu},T)/I_o(\tilde{\nu},T)$, where $I(\tilde{\nu},T)$ and $I_o(\tilde{\nu},T)$ are the intensities of the sample and background spectra, respectively. Napierian absorbance spectra $A_{obs}(\tilde{\nu},T)$ were calculated from the transmittance data as: $A_{obs}(\tilde{\nu},T)=-\ln\{\tau(\tilde{\nu},T)\}$.

The r.m.s. signal-to-noise ratio in each of the transmittance spectra exceeded 1000:1 across the entire spectral range of the water vapour absorption features, giving an information-to-noise ratio in excess of 100:1 for absorbances between 0.2 and 3.5. The maximum information-to-noise ratio at an absorbance of around 1.0 was 370:1.

3. RESULTS AND DISCUSSION

(a) Preliminary data treatment

The observed laboratory spectra were compared with calculated absorbance spectra, generated for the measured laboratory conditions using HITRAN v.11 (http://www.hitran.com; Rothman *et al.* 2003), the line-by-line (LBL) code of Mitsel *et al.* (1995), and the Reference Forward Model (RFM) line-by-line code of Dudhia (1997). Detailed information about the optical configuration of the FTS and the numerical apodisation function was used to calculate a wavelength-dependent instrument line shape and convolute it then with the calculated molecular spectrum.

An example of the initial residual between optical depth derived from experiment and the calculated WM optical depth, including the CKD-2.4 water vapour continuum, is shown in the Fig. 2(a). The residual is presented with a spectral resolution of 5 cm^{-1}.

It should be mentioned that there is no significant difference between HITRAN-96 and HITRAN v.11 for H_2O spectral lines in the spectral region 3500-6000 cm^{-1} (see for example Ptashnik and Shine (2003)). It means that using CKD-2.4 with HITRAN v.11 is quite justified in this case, in spite of the fact that originally HITRAN-96 is supposed to be used with this version of CKD continuum.

To calculate the residual, only parts of the spectrum (both measured and calculated) below an optical depth threshold (ODT) of 2 were used, to exclude the impact of regions of the spectrum which are saturated. Such a method of data processing does not affect the continuum part of the residual we are interested in here, because for both measurement conditions this part is much less than the threshold level.

The bars in the Fig. 2(a) show only experimental error. However, there are two other main sources of error, which should be taken into account to get the final residual.

1) Uncertainty of spectral line parameters:

It was found that any systematic error in the initial HITRAN lines parameters, for example a 15% error either in line intensity *S* or self-broadening halfwidth parameter γ^{o}_{self}, could lead to a similar shape and size of the residual shown in Fig. 2(a). This is especially important, as HITRAN does not have the information about self-broadening parameters for this spectral region. In such circumstances line-by-line codes usually use

the approximation $\gamma^{o}_{self} = k \cdot \gamma^{o}_{air}$, where γ^{o}_{air} is the air-broadening coefficient, and $k \sim 5$. While this approximation is not normally serious for atmospheric calculations, where air broadening prevails, it is of much greater importance when interpreting pure water spectra in laboratory conditions.

To exclude the possibility that such errors were the cause of the residual we decided to derive γ^{o}_{self} and the line intensity parameters by fitting the calculated spectrum to the measured one. The measured spectrum for water vapour pressure 20 hPa and path length 29 cm was used to fit parameters of the 460 strongest lines ($S > 2\times10^{-23}$ cm mol^{-1}) in this spectral region that, as was found from numerical experiment, are most important when computing the residual. We used the Levenberg-Marquardt least square algorithm to fit 3 parameters (centre position, intensity, and self-broadening coefficient) for each spectral line. The Voigt profile was used for the fitting. Additionally the baseline was fitted for every 3 consecutive spectral lines. The mean error of the S and γ^{o}_{self} parameters determination was estimated to be about 5%.

Figure 3 shows parts of measured high spectral resolution spectrum compared with the calculation using HITRAN and the modified HITRAN (we will refer to this database with newly fitted lines as 'modified-HITRAN' or 'HITRAN(m)'). Fig. 2(b) displays the correction that should be subtracted from the initial residual (Fig. 2(a)), to take into account the impact of the new line parameters. Comparison of Figs 2(a) and 2(b) shows that the impact of the correction of line parameters on the original residual is significant and accounts for much of the residual at wavenumbers above 5500 cm^{-1} and below 5150 cm^{-1}. This indicates the importance of a careful assessment of the quality of line parameters in this work. The other details of the line fitting, as well as the fitted line parameters will be reported separately. They can be found in HITRAN format at the British Atmospheric Data Centre (http://badc.nerc.ac.uk/data/cwvc/hitran /index.html).

To minimise the possible impact of parameter errors in weaker ($S < 2\times10^{-23}$ cm mol^{-1}) unfitted HITRAN lines, we did not include in the residual calculation (in addition to the ODT limitation mentioned above) parts of the spectra (both, measured and calculated) near the centres of these lines. The width of the cut-off areas was derived so that the line contribution was less then 5% of the maximum residual value. Such an approach is quite reasonable when we are interested only in the smooth (continual) part of the residual. Taking into account that the maximum cut-off distance (for the strongest of the unfitted lines) that satisfies the 5% requirement is about 0.3 cm^{-1} for 20 hPa and 0.6 cm^{-1} for 98 hPa measurement respectively, we have got still enough data points in the each 5 cm^{-1} spectral region to be processed.

2) Weak lines contribution:

HITRAN does not include parameters of very weak lines ($S < 10^{-26}$-10^{-27} cm mol^{-1}). Schwenke and Partridge (2000) have recently updated their *ab initio* calculation of water vapour line parameters (Partridge and Schwenke 1997), which include such weak lines, and allows an estimation of their contribution. To assess the impact of these weak lines it is necessary to account for the fact that many of the lines in the Partridge-Schwenke (hereafter PS) database are also in HITRAN. There are several possible ways in which the weak line contribution can be estimated (see Ptashnik and Shine 2003). We believe that the best method is to replace all the lines in the PS database by their HITRAN equivalent, if they have one; this ensures that differences between the PS and HITRAN databases are solely due to lines which are uncatalogued on HITRAN, rather than because of differences in spectral parameters of catalogued lines between PS and HITRAN. This is the PS ← HITRAN case of Ptashnik and Shine (2003).

Figure 2(c) shows the contribution of the PS weak lines, where it can be seen to be generally significantly smaller than the residual in Fig. 2(a).

It should be mentioned again that only those parts of corrections due to line parameters fitting and PS weak lines, which are below the ODT = 2 are presented in Figs 2(b) and (c). The total weak lines contribution (i.e. without using ODT) is several times larger.

(b) Water dimer as a "separate" absorber

The corrected optical depth residual, which takes into account the new line parameters, the weak lines and CKD-2.4 continuum is shown in Fig. 4 together with the expected dimer absorption. Error bars include in this case both the measurement error and estimated uncertainty (standard deviation) caused by error in the line parameters fitting. Two WD parameters, K_{eq} and HWHM, were fitted to best match the central (bigger) peak of the residual (near 5340 cm^{-1}). K_{eq} was found to be 0.018 ± 0.003 and 0.011 ± 0.0025 atm^{-1} for the 20 hPa, 299 K, and for 98 hPa, 342 K measurement respectively, whereas the mean HWHM value is found to be 18 ± 3 cm^{-1}.

To be in best agreement with the residual, the $|0\rangle_f|1\rangle_b|1\rangle$ and two close (unresolved) $|10\rangle\_|1\rangle$ and $|1\rangle_f|0\rangle_b|1\rangle$ stretching+bending WD bands (using Schofield and Kjaergaard's (2003) notation) are red-shifted in Fig. 4 with respect to their positions predicted by Schofield and Kjaergaard (2003) (5231, 5341 and 5357 cm^{-1} respectively) by 12 cm^{-1} (Fig. 4(a)) and 5 cm^{-1} (Fig. 4(b)). These shifts are much less than the uncertainty of the prediction. The Perchard's (2001) low temperature experimental study of the water trapped in a nitrogen matrix has revealed the $|10\rangle\_|1\rangle$ WD band to be positioned near 5296 cm^{-1}, indicating that there is uncertainty in the precise position of the WD bands, which can also depend on the ambient conditions.

Taking also into account uncertainty in the knowledge of the main WD parameters, quite good agreement between residuals and expected WD signatures can be seen for both measurements, apart from the part of the residual between 5400 and 5500 cm^{-1}. This part can be attributed either to extra CKD continuum or non-predicted WD or higher order water clusters absorption features (for example, trimers). The higher-order cluster explanation may be favoured because of the stronger dependence on p_{H2O} than is the case for the dimer, as can be seen for this part of the residual if one to compare Fig.4 (a) and (b).

(c) Water dimer as a part of CKD continuum

An alternative interpretation of the residual and its relationship with the expected dimer absorption can be suggested. Taking into account that the CKD continuum is a semi-empirical model, which has been fitted to observation in only some parts of the spectrum (Clough *et al.* 1989; Mlawer *et al.* 1999), we can suggest that it may contain absorption of some other components (in addition to the WM line far wings), such as water dimers. In spite of the fact that no experimental data in the spectral region under our investigation was used for CKD parameters fitting, these parameters could include some WD contribution through the presence of WD absorption in the spectral regions where the CKD parameters were fitted (for example, below 2500 cm^{-1}).

Figure 5 shows the residual between measurement and modified-HITRAN calculation using Ma and Tipping (1999, 2002) (MT) continuum included instead of CKD. The MT continuum model is distinct from CKD model in the sense that it is based on far wing line shape theory, which does not rely on adjustable parameters or fitting to observation; thus, it cannot include any other components in addition to the far wing contribution. It can be seen from Fig. 5 that the MT continuum is about 4 times less than CKD in this spectral region. The value of WD equilibrium constant that best matches the residual in this case was found to be $K_{eq} = 0.043 \pm 0.0055$ atm^{-1} for 299 K, 20 hPa, and $K_{eq} = 0.02 \pm 0.0035$ atm^{-1} for 342 K, 98 hPa, and therefore significantly higher than

the values derived in section 3(b). The mean value of the WD band HWHM=28±4 cm^{-1} matches the central residual peak quite well.

Again, the residual in the spectral region 5400 - 5500 cm^{-1} cannot be explained either by the MT continuum or by the present WD feature. The WD band shifts in the Fig. 5 are similar to those obtained in Fig. 4.

(d) Implication for the dimerization equilibrium constant

Figure 6 displays two sets of K_{eq} we have obtained, together with several other calculated and experimentally derived values of water dimerization equilibrium constant. It is clear from the plot that our upper estimation of K_{eq} temperature dependence ($K_{eq.up}(T)$), derived from the residual 'Measurement – HITRAN(m)_with_ MT_continuum', is in much better agreement with the Curtiss et al. (1979) measurements and extrapolation, than the lower $K_{eq.low}(T)$ estimation, which was obtained from the residual with CKD continuum subtracted. The $K_{eq.up}(T)$ is also very close to the Slanina and Crifo (1992) calculations and is in a very good agreement with the $K_{eq}(292.4\ K)=0.05\ atm^{-1}$, derived by Pfeilsticker *et al.* (2003)[2] (K.Pfeilsticker, personal communication, 2003) in an independent measurement and in a rather different spectral region. However, both the Pfeilsticker *et al.* (2003) and our measurements do not support the Goldman *et al.* (2001) prediction of the strong K_{eq} dependence on temperature (Fig. 6). Munoz-Caro and Nino (1997) explain the low values of their calculated $K_{eq}(T)$ (Fig. 6) by the lack of interaction in the vibrational model they used.

The low set of our K_{eq} estimation, when combined with the Curtiss *et al.* (1979) experimental data points, by contrast, shows very small, nearly zero, temperature dependence, which is in contradiction with all theoretical predictions. This all indicates that WD absorption is, most probably, included partly/mostly in the modern CKD continuum model (self-broadening part) through the fitting of CKD continuum parameters to the experimental data, which included some component of WD absorption. Taking into account that WDs can be regarded, to some degree, as colliding water molecules with very long collision duration, the contribution of water dimer absorption can cause the 'chi-function' correction in CKD continuum (Clough *et al.* 1989) very similar to the one caused by deviation from the impact collision model.

(e) Implication for shortwave absorption by the atmosphere

Vaida *et al.* (2001) have shown that the spectral regions 4000-5000 cm^{-1} and 5600-6500 cm^{-1} should give the main contribution to WD shortwave absorption. This contribution is caused mainly by far wings of the $|0\rangle_f|1\rangle_b|0\rangle$, $|1\rangle_f|0\rangle_b|0\rangle$ and $|10\rangle\_|0\rangle$ WD bands, centred near 3600, 3730 and 3745 cm^{-1}, and by wings of $|0\rangle_f|1\rangle_b|1\rangle$, $|10\rangle\_|1\rangle$ and $|1\rangle_f|0\rangle_b|1\rangle$ bands, centred near 5230, 5340 and 5357 cm^{-1} respectively. We applied our derived values of WD bandwidth and Lorentzian line shape to all WD bands and used this approximation, together with the derived sets of K_{eq} and Schofield and Kjaergaard (2003) WD spectroscopic information, to estimate the global mean extra shortwave absorption, caused by WD.

The fast line-by-line code of Mitsel *et al.* (1995) was used for high (0.001 cm^{-1}) spectral resolution calculation of optical depth for each of 17 atmospheric layers of

---

[2] $K_{eq}(292.4\ K) = 0.047\ atm^{-1}$ was obtained from the experiment, assuming the band intensity calculated by Low and Kjaergaard (1999), $S = 3.04\times10^{-22}$ cm $molec^{-1}$. This corresponds to $K_{eq}= 0.05\ atm^{-1}$ if the more recent Schofield and Kjaergaard (2003) calculated value of $S = 2.84\times10^{-22}$ cm $molec^{-1}$ is used for the same band.

clear-sky mid-season zonal-mean atmospheric profiles at a latitudinal resolution of 10°. Apart from the H_2O monomer and dimer, the model also includes CO_2, O_3, CH_4 and O_2. The optical depth spectra were used then as input to the Discrete Ordinate (DISORT) code of Stamnes *et al.* (1988) for irradiance calculations. Rayleigh scattering was taken into account using DISORT with 4-streams approximation. The solar irradiance at the top of the atmosphere compiled by Kurucz (1998) is employed, which presents the solar spectrum at the spectral resolution of 1 cm^{-1} (total solar irradiance = 1368.8 Wm^{-2}).

The WD partial pressure profiles for each atmospheric WM profile was calculated from equation (2). We used the value ΔH_{up}= -3.78 kcal mol^{-1} and ΔS_{up}= -18.89 cal $K^{-1}mol^{-1}$ in equation (1) to interpolate/extrapolate our $K_{eq\cdot up}(T)$ and Curtiss *et al.* (1979) data to atmospheric temperatures (upper dash-dotted line in Fig. 6). These values are very close to those, derived by Curtiss *et al.* (1979) (ΔH= -3.59 ± 0.5 kcal mol^{-1} and ΔS= -18.59 ± 1.3 cal $K^{-1}mol^{-1}$). Similarly, the values ΔH_{low}= -1.590 kcal mol^{-1} and ΔS_{low}= -13.29 cal $K^{-1}mol^{-1}$ were used to extrapolate/interpolate the $K_{eq\cdot low}(T)$ together with Curtiss *et al.* (1979) data (lower dash-dotted line in Fig. 6). However, these ΔH and ΔS values are too far from those derived by different authors (see Curtiss *et al.* 1979); thus, they can only be regarded as fitting parameters of our investigation.

In Fig. 7 the calculated latitudinal dependence of WD absorption of solar irradiance in the spectral region 1500-17000 cm^{-1} is presented for March - May for both sets of the K_{eq} and HWHM obtained. For the other seasons the dependences look similar, apart from a ±10° shift for the winter and summer seasons respectively. The global mean value of extra absorption due to WD is ~0.42 Wm^{-2} (for the $K_{eq.low}$ and HWHM=18 cm^{-1}) and ~1.5 Wm^{-2} (for the $K_{eq.up}$ and HWHM=28 cm^{-1}), or about 0.5% and 2% of the total clear-sky absorption respectively. Calculation with the Curtiss *et al.* (1979) extrapolation of $K_{eq}(T)$ (dashed line in Fig. 6) with HWHM=28 cm^{-1} gives ~1.3 Wm^{-2} global mean WD absorption.

Figure 8 displays the calculated spectrum of the solar direct flux at surface and WD contribution to the flux for a tropical atmosphere case overhead sun, for a column water vapour amount of 47 kg m^{-2}. The dashed lines display the cumulative WD absorption (i.e. the extra absorption integrated from 1500 cm^{-1} to the given wavenumber) that reaches 2 Wm^{-2} and 7.2 Wm^{-2} for low and upper set of the $K_{eq}(T)$ respectively. The latter value is about twice higher than the upper estimate of Vaida *et al.* (2001), which is caused mainly by the fact that our K_{eq} is ~2 times bigger. Chylek *et al.* (1999) estimate of WD absorption 6 Wm^{-2} for tropical atmosphere, by contrast, is very close to ours. However, this is largely coincidental as their value is obtained with a value of K_{eq} approximately 3.5 times lower than ours, which reflects the fact that WD overtone intensities predicted by Tso *et al.* (1998) are significantly larger than the ones calculated by Schofield and Kjaergaard (2003).

Figure 8 shows that the main contribution to the extra absorption comes from the wings of the WD bands referred above, rather than from the band centres. Figure 1 indicates that the CKD-2.4 continuum is much weaker than the theoretical estimates of the WD absorption in these wings. Therefore, even if CKD-2.4 is included in radiation budget calculations, the extra absorption due to WD is more likely to be closer to our upper estimate, assuming that the Lorentzian approximation of the WD bands is valid.

Finally, in Fig. 9 the calculated atmospheric heating rate due to WD absorption is presented for the mid-latitude summer profile (Ellingson *et al.* 1991). It can be seen that the main WD contribution to shortwave absorption appears near the surface. It is caused by the fact that the quadratic dependence of WD amount on that of WM (Eq. 2) is stronger than the growth of $K_{eq}(T)$ when temperature falls with height.

It is worth reiterating that all assessments of WD absorption are highly dependent on the widths and far wing shapes of the strongest WD bands, centred near 3600, 3730 and 3745 cm^{-1}. For example, decreasing the HWHM of these 3 bands alone from the values of 28 and 18 cm^{-1}, used here, to ~6 cm^{-1} (Huisken *et al* .1996) will decrease all WD absorption values, presented in the Figs.7-9, by a factor 2 to 2.5.

4. CONCLUSION

In spite of the quite strong overlapping lines of the water monomer, a quasi-continual residual absorption, very similar to that expected from the water dimer $|0\rangle_f|1\rangle_b|1\rangle$, $|10\rangle\_|1\rangle$ and $|1\rangle_f|0\rangle_b|1\rangle$ stretching+bending combination bands, was observed in a series of laboratory measurements for different pressures and temperatures in the spectral region 5000-5600 cm^{-1}. The measured residuals have a 5-10 cm^{-1} red shift in comparison with the Schofield and Kjaergaard (2003) theoretical prediction. The dimerization equilibrium constants (K_{eq}(299 K) = 0.043±0.0055 atm^{-1} and K_{eq}(342 K) = 0.02±0.0035 atm^{-1}), derived from the residual 'Measurement – modified_HITRAN_ with_Ma&Tipping_continuum' are in a good agreement with the main theoretical predictions and with all experimental observations of the value. It can mean that a substantial part of water dimer absorption is, most probably, already included as part of the present self-broadening CKD continuum model, at least near the band centres. The lower and upper estimation of water dimer contribution to the global-mean solar radiation absorption is found to be about 0.5% and 2% of the total atmospheric absorption. However, on the basis of a comparison of the derived K_{eq} values with others in the literature we believe that dimer contribution is closer to the higher estimate. Our upper limit is 2-2.5 times bigger than the upper estimation of Vaida *et al.* (2001); however, it is much less than would follow from the Goldman *et al.* (2001) calculation of water dimerization equilibrium constant.

On the basis of the latest Schofield and Kjaergaard (2003) calculation it can be suggested that the largest water dimer contribution to the water vapour continuum should be expected from the strongest water dimer's bands $|0\rangle_f|1\rangle_b|0\rangle$, $|1\rangle_f|0\rangle_b|0\rangle$ and $|10\rangle\_|0\rangle$ near 3700 cm^{-1} (see Fig. 1). However, for atmospheric radiation budget applications it seems more important to investigate the absorption/shape of the *far wings* of these WD bands, as well as the bands investigated in our work. The far wing absorption of these bands gives the main contribution to water dimer global radiative impact. The Lorentzian wing approximation for the water dimer bands, used in our work (and, for example, in the work of Vaida *et al.* 2001), should be regarded probably as a first approximation, and can be a source of significant uncertainty when estimating the water dimer absorption (see also Kjaergaard *et al.* 2003).

An additional absorption was registered in the spectral region 5400-5500 cm^{-1} that cannot be explained either by CKD-2.4 water continuum, or by the currently predicted water dimer spectrum.

ACKNOWLEGEMENTS

We are very grateful to Henrik Kjaergaard, Eli Mlawer, Klaus Pfeilsticker, Richard Tipping, Anu Dudhia, Boris Fomin, Olga Naumenko and Ahilleas Maurellis for fruitful discussions and help in providing us with up-to-date datasets. The authors thank the UK Natural Environment Research Council (Grants NER/T/S/2000/00982, NER/T/S/2001/00194 and NER/T/S/2001/01117) for support and the technical assistance of R. G. Williams at the Rutherford Appleton Laboratory Molecular Spectroscopy Facility.

REFERENCES

Arking, A. 1999 Bringing climate models into agreement with observations of atmospheric absorption. *J. Clim.*, **12**, 1589–1600

Ballard, J., Strong, K., Remedios, J., Page, M. and Johnston, W. B. 1994 A coolable long path absorption cell for laboratory spectroscopic studies of gases. *J. Quant. Spectrosc. Radiat. Transfer*, **52**, 677-691

Chylek, P., Fu, Q., Tso, H.C.W. and Geldart, D.J.W. 1999 Contribution of water vapor dimers to clear sky absorption of solar radiation. *Tellus*, **51A**, 304-313

Clough, S.A., Kneizys, F.X. and Davies, R.W. 1989 Line shape and water vapor continuum, *Atmos. Res.*, **23**, 229–241

Conant, W.C., Vogelmann, A.M. and Ramanathan, V. 1998 The unexpected solar absorption and atmospheric H_2O: a direct test using clear-sky data. *Tellus*, **50A**, 525-533

Curtiss, L.A., Frurip, D.J. and Blander, M. 1979 Studies of molecular association in H_2O and D_2O vapors by measurement of thermal conductivity. *J. Chem. Phys.*, **71**, 2703-2711

Daniel, J.S., Solomon, S., Sanders, R.W., Portmann, R.W. and Miller, D.C. 1999 Implication for water monomer and dimer solar absorption from observations at Boulder, Colorado. *J. Geophys. Res.*, **104**, 16785-16791

Devir, A.D., Neumann, M., Lipson, S.G. and Oppenheim, Uri P. 1994 Water vapor continuum in the 15- to 25-μm spectral region: Evidence for $(H_2O)_2$ in the atmosphere. *Optical Engineering*, **33**, 746-750

Dudhia, A. 1997 Reference forward model version 3: Software user's manual. *Eur. Space Technol. Cent. (ESTEC) Document PO-MA-OXF-GS-0003*, Eur. Space Agency (ESA), Paris, France

Ellingson, R.G., Ellis, J. and Fels, S. 1991 The intercomparison of radiation codes used in climate models: Longwave results. *J. Geophys. Res.*, **96**, 8929-8953

Evans, G.T. and Vaida, V. 2000 Aggregation of water molecules: Atmospheric implications. *J. Chem. Phys.*, **113**, 6652-6659

Goldman, N., Fellers, R.S., Leforestier, C. and Saykally, J. 2001 Water dimers in the atmosphere: Equilibrium constant for water dimerization from the VRT(ASP-W) potential surface. *J. Phys. Chem.*, **105**, 515-519

Headrick, J.E. and Vaida, V. 2001 Significance of water complexes in the atmosphere. *Phys. Chem. Earth I*, **26**, 479-486

Hill, C. and Jones, R. 2000 Absorption of solar radiation by water vapor in clear and cloudy skies: Implications for anomalous absorption. *J. Geophys. Res.*, **105**, 9421-9428

Huang, Z.S. and Miller, R.E. 1989 High-resolution near infrared spectroscopy of water dimer. *J. Chem. Phys.*, **91**, 6613-6631

Huisken, F., Kaloudis, M. and Kulcke, A. 1996 Infrared spectroscopy of small size-selected water clusters. *J. Chem. Phys.*, **104**, 17-25

Kato, S., Ackerman, T.P., Clothiaux, E.E., Mather, J.H., Mace, G.G., Wesley, M.L., Murcray, F. and Michalsky, J. 1997 Uncertainties in modelled and measured clear-sky surface shortwave irradiances. *J. Geophys. Res.*, **102**, 25881-25898

Kurucz, R.L.	1998	http://cfaku5.harvard.edu/sun/irradiance/
Kjaergaard, H.G., Robinson, T.W., Howard, D.L., Daniel, J.S., Headrick J.E. and Vaida, V.	2003	Complexes of Importance to the Absorption of Solar Radiation. *J. Phys. Chem. A*, **107**, 10680–10686
Low, G.R. and Kjaergaard, H.G.	1999	Calculation of OH-stretching band intensities of the water dimer and trimer. *J. Chem. Phys.*, **110**, 9104-9115
Ma, Q. and Tipping, R.H.	1999	The averaged density matrix in the coordinate representation: Application to the Calculation of the far-wing line shape for H_2O. *J. Chem. Phys.*, **111**, 5909
	2002	The frequency detuning correction and the asymmetry of line shapes: The far wing of H2O-H2O. *J. Chem. Phys.*, **116**, 4102-4115.
Mertz, L.	1967	Auxillary computation for Fourier transform spectrometry. *Infrared Phys.* **7**, 17-23
Mhin, B.J., Lee, S.J. and Kim, K.S.	1993	Water-cluster distribution with respect to pressure and temperature in the gas phase. *Phys. Rev. A*, **48**, 3764-3770
Mitsel, A.A., Ptashnik, I.V., Firsov, K.M. and Fomin, A.B.	1995	Efficient technique for line-by-line calculating the transmittance of the absorbing atmosphere. *Atmos. Oceanic Opt.*, **8**, 847–850
Mlawer, E.J., Clough, S.A., Brown, P.D. and Tobin, D.C.	1999	Recent developments in the water vapor continuum. *Ninth ARM Science Team Meeting Proceedings*, pp. 1–6, March 22-26, San Antonio, TX
Munoz-Caro, C. and Nino, A.	1997	Effect of anharmonicities on the thermodynamic properties of the water dimer. *J. Phys. Chem.*, **101**, 4128-4135
Norton, R. H. and Beer, R.	1976	New apodizing functions for Fourier spectrometry. *J. Opt. Soc. Am.,* **66**, 259-264
Partridge, H. and Schwenke, D.W.	1997	The determination of an accurate isotope potential energy surface for water from extensive ab-initio calculation and experimental data. *J. Chem. Phys.*, **106**, 4618–4639
Paul, J.B, Collier, C.P., Saykally, R.J., Scherer, J.J. and O'Keefe, A.	1997	Direct measurement of water cluster concentration by infrared cavity ringdown laser absorption spectroscopy. *J. Phys. Chem. A*., **101**, 5211-5214
Penner, S.S. and Varanasi P.	1967	Spectral absorption coefficient in the pure rotational spectrum of water vapor. *J.Quant. Spectrosc. Radiat. Transfer*, **7**, 687-690
Perchard, J.P.	2001	Anharmonicity and hydrogen bonding. II – A near infrared study of water trapped in nitrogen matrix. *Chem. Phys.*, **266**, 109-124
Pfeilsticker, K., Lotter, A., Peters, C. and Bosch, H.	2003	Atmospheric detection of water dimers via near-infrared absorption. *Science*, **300**, 2078-2080
Pilewskie, P., Rabbette, M., Bergstrom, R., Marquez, J., Schmid, B. and Russell, P.B.	2000	The discrepancy between measured and modelled downwelling solar irradiance at the ground: Dependence on water vapor. *Geophys. Res. Lett.*, **27**, 137-140

Ptashnik, I.V. and Shine, K.P.	2003	Calculation of solar radiative fluxes in the atmosphere: The effect of updates in spectroscopic data. *Atmos. Oceanic Opt.*, **16**, 251-255
Ramanathan, V. and Vogelmann, A.M.	1997	Greenhouse effect, atmospheric solar absorption and the Earth's radiation budget: From Arrhenius-Langley era to the 1990s. *Ambio*, **26**, 38-46
Remedios, J. J.	1990	D. Phil.Thesis, Oxford University
Rothman, L.S., Barbe, A., Chris Benner, D., Brown, L.R., Camy-Peyret, C., Carleer, M.R., Chance, K., Clerbaux, C., Dana, V., Devi, V.M., Fayt, A., Flaud, J.-M., Gamache, R.R., Goldman, A., Jacquemart, D., Jucks, K.W., Lafferty, W.J., Mandin, J.-Y., Massie, S.T., Nemtchinov, V., Newnham, D.A., Perrin, A., Rinsland, C.P., Schroeder, J., Smith, K.M., Smith, M.A.H., Tang, K., Toth, R.A., Vander Auwera, J., Varanasi, P. and Yoshino, K.	2003	The HITRAN molecular spectroscopic database: edition of 2000 including updates through 2001. *J. Quant. Spectrosc. Radiat. Trans.* **82**, 5-44
Schofield, D.P. and Kjaergaard, H.G.	2003	Calculated OH-stretching and HOH-bending vibrational transitions in the water dimer. *Phys. Chem. Chem. Phys.*, **5**, 3100-3105
Schwenke, D.W. and Partridge, H.	2000	Convergence testing of the analytic representation of an ab-initio dipole moment function for water: Improved fitting yields improved intensities. *J. Chem. Phys.*, **113**, 6592–6597
Slanina, Z. and Crifo, J.-F.	1992	A refined evaluation of the gas-phase water-dimerization equilibrium constant within nonrigid BJH- and MCY-type potentials. *Int. J. Thermophys*. **13**, 465-476
Smith, K.M., Ptashnik, I.V., Newnham, D.A. and Shine, K.P.	2004	Absorption by water vapour in the 1 to 2μm region. *J. Quant. Spectrosc. Radiat. Trans.*, **83**, 735-749
Stamnes, K., Tsay, S.C., Wiscombe, W. and Jayaweera, K.	1988	A numerically stable algorithm for Discrete-Ordinate-Method transfer in multiply scattering and emitting layered media, *Appl. Opt.*, **27**, 2502-2509
Tso, H.C.W., Geldart, D.J. and Chylek, P.	1998	Anharmonicity and cross section for absorption of radiation by water dimer. *J. Chem. Phys.*, **108**, 5319-5329
Vaida, V., Daniel, J.S., Kjaergaard, H.G., Goss, L.M. and Tuck, A.F.	2001	Atmospheric absorption of near infrared and visible solar radiation by the hydrogen bonded water dimer. *Q.J.R. Meteorol. Soc.*, **127**, 1627-1643
Vaida, V. and Headrick, J.E.	2000	Physicochemical Properties of Hydrated Complexes in the Earth's Atmosphere. *J. Phys. Chem. A*, **104**, 5101-5412

CAPTIONS

Figure 1. Optical depth of the water monomer including CKD-2.4 continuum, two recent theoretical estimates for the water dimer and CKD-2.4 self-broadening continuum separately, for optical path length 10 m, pure water vapour pressure 15 hPa, and T=293 K. The dimer absorption band's HWHM=25 cm^{-1} (Lorentzian profile) and the dimerization equilibrium constant $K_{eq} = 0.041$ atm^{-1} are used for the dimer calculation.

Figure 2. (a) Initial view of the residual optical depth for 20 hPa, 128 m and 299 K experiment. Spectral resolution is 5 cm^{-1}. (b) Contribution to the residual in (a) that should be subtracted, because of the new spectral line parameters fitting. (c) Contribution that should be subtracted from the residual because of the impact of weak lines. Thick lines in (a) and (b) show 5 points smoothing.

Figure 3. Example of comparison the calculated optical depth using HITRAN (v.11) and modified-HITRAN (new line parameters) and the measured one, for the pure water pressure 20 hPa, path length 29 cm and temperature 297 K.

Figure 4. Corrected residual between measurement and modified-HITRAN calculations with CKD-2.4 included. Bars show the measurement errors and errors of spectral line parameters fitting. (a) 20 hPa, 128 m, 299 K measurement. (b) 98 hPa, 9.7 m, 342 K measurement. To best fit the residual, the dimer spectrum is red-shifted by 12 cm^{-1} and 5 cm^{-1} for (a) and (b) respectively.

Figure 5. Corrected residual between measurement and modified-HITRAN calculations with Ma and Tipping continuum included. Bars show the measurement errors and errors of spectral line parameters fitting. (a) 20 hPa, 128 m, 299 K measurement. (b) 98 hPa, 9.7 m, 342 K measurement. To best fit the residual, the dimer spectrum is red-shifted by 9 cm^{-1} and 5 cm^{-1} for (a) and (b) respectively.

Figure 6. Different theoretical and experimental determinations of the $K_{eq}(T)$ dependence including the current work. The shaded area shows the uncertainty of Curtiss *et al.* (1979) extrapolation caused by experimental and calculation errors. The dash-dotted lines display the temperature interpolation/extrapolation of the lower and upper set of the K_{eq} derived in this paper.

Figure 7. The latitudinal dependence of water dimer solar absorption in the spectral region 1500-17000 cm^{-1} for March-May for the lower and upper set of the K_{eq} derived in this paper.

Figure 8. The calculated spectrum of the solar direct flux at the surface and water dimer spectral and cumulative (right axis) contribution to the absorption for an overhead sun in a tropical atmosphere. The upper and lower curves for the water dimer absorption correspond to the upper and lower sets of K_{eq}.

Figure 9. The calculated atmospheric heating rate due to WD absorption (lower and upper estimate) for the mid-latitude summer ICRCCM atmospheric profile and solar zenith angle of 30°.

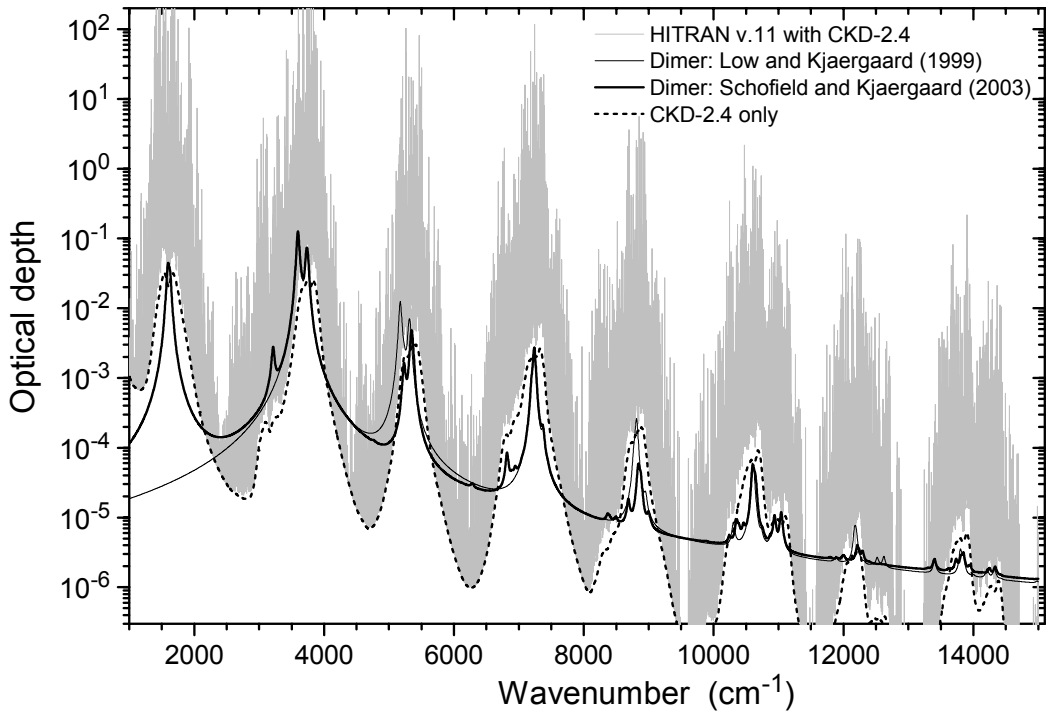
HITRAN v.11 with CKD-2.4
Dimer: Low and Kjaergaard (1999)
Dimer: Schofield and Kjaergaard (2003)
CKD-2.4 only
Optical depth
Wavenumber (cm-1)
10^2
10^1
10^0
10^-1
10^-2
10^-3
10^-4
10^-5
10^-6
2000
4000
6000
8000
10000
12000
14000

Figure 1.

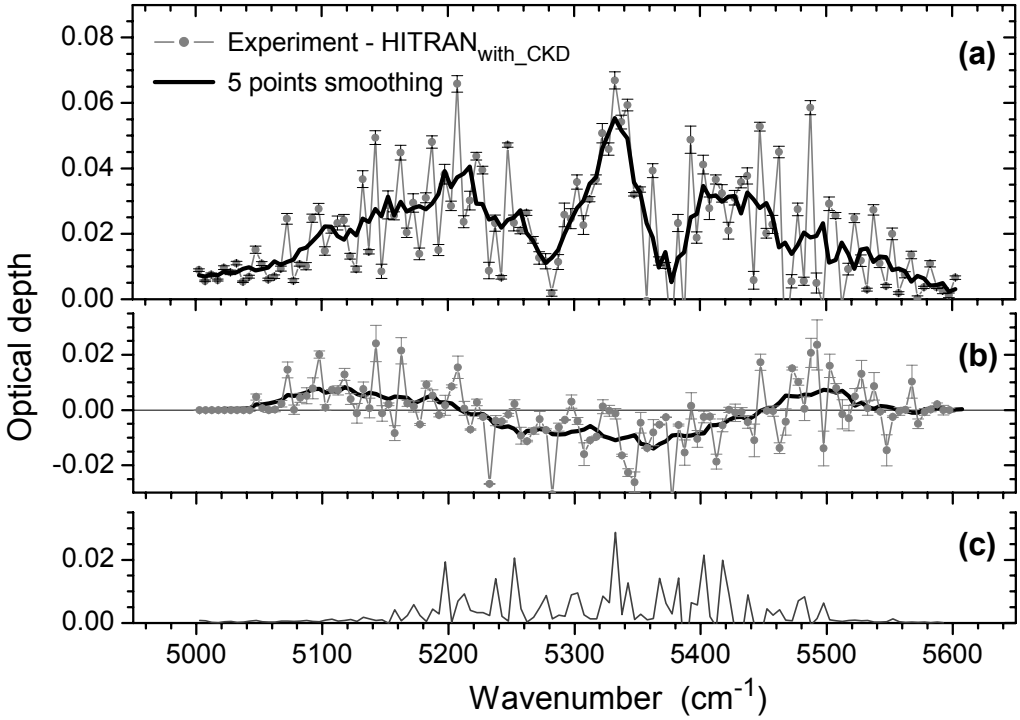

Figure 2.

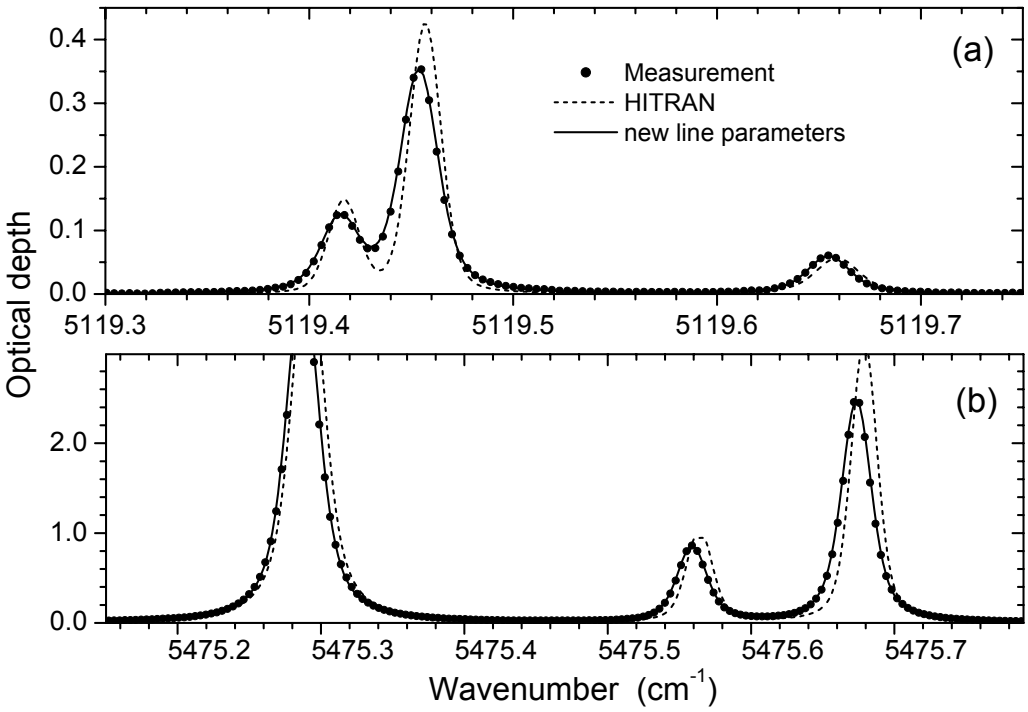

Figure 3.

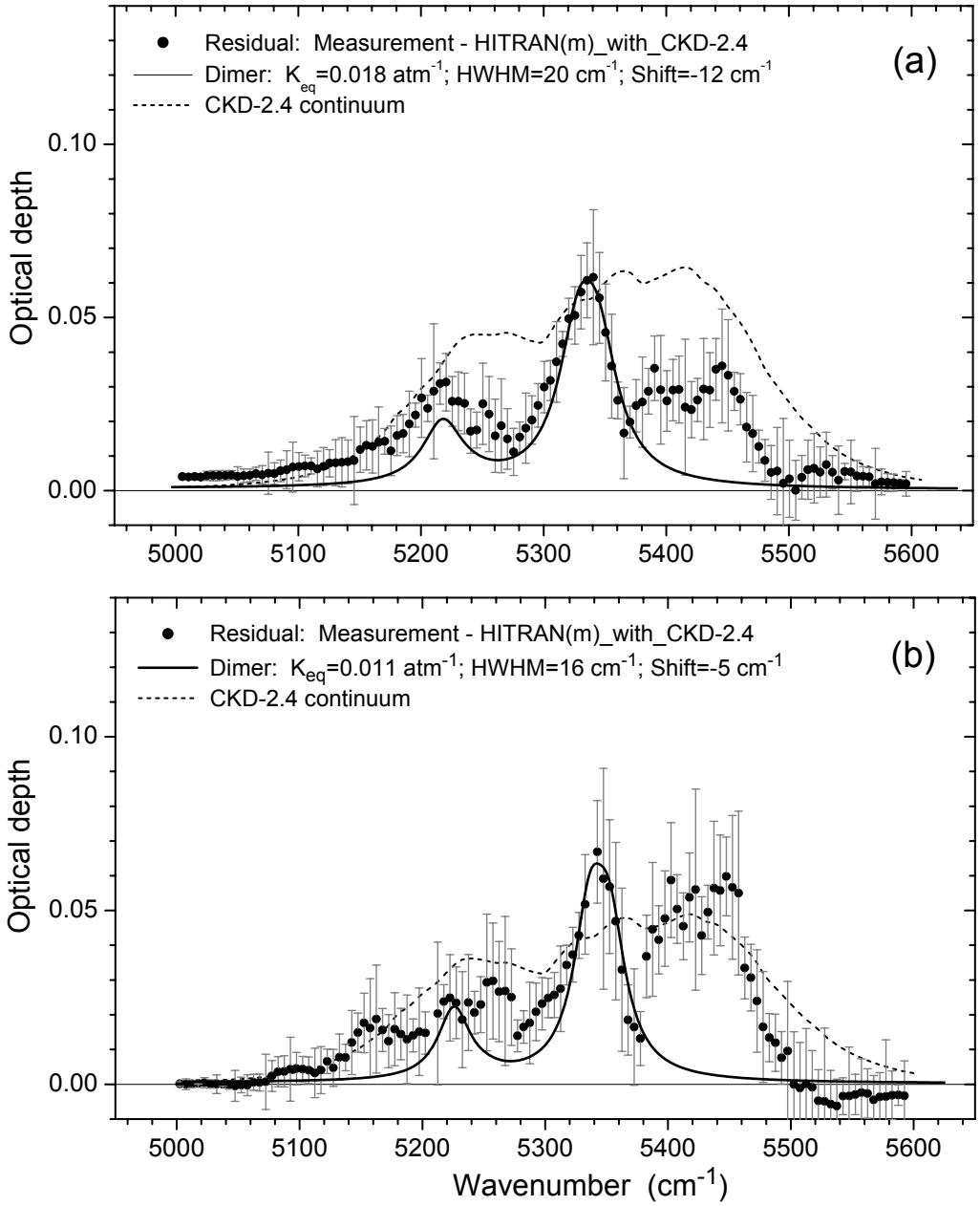
Residual: Measurement - HITRAN(m)_with_CKD-2.4
Dimer: K_{eq}=0.018 atm^{-1}; HWHM=20 cm^{-1}; Shift=-12 cm^{-1}
CKD-2.4 continuum
(a)
Optical depth
0.10
0.05
0.00
5000
5100
5200
5300
5400
5500
5600
Residual: Measurement - HITRAN(m)_with_CKD-2.4
Dimer: K_{eq}=0.011 atm^{-1}; HWHM=16 cm^{-1}; Shift=-5 cm^{-1}
CKD-2.4 continuum
(b)
Optical depth
0.10
0.05
0.00
5000
5100
5200
5300
5400
5500
5600
Wavenumber (cm^{-1})

Figure 4.

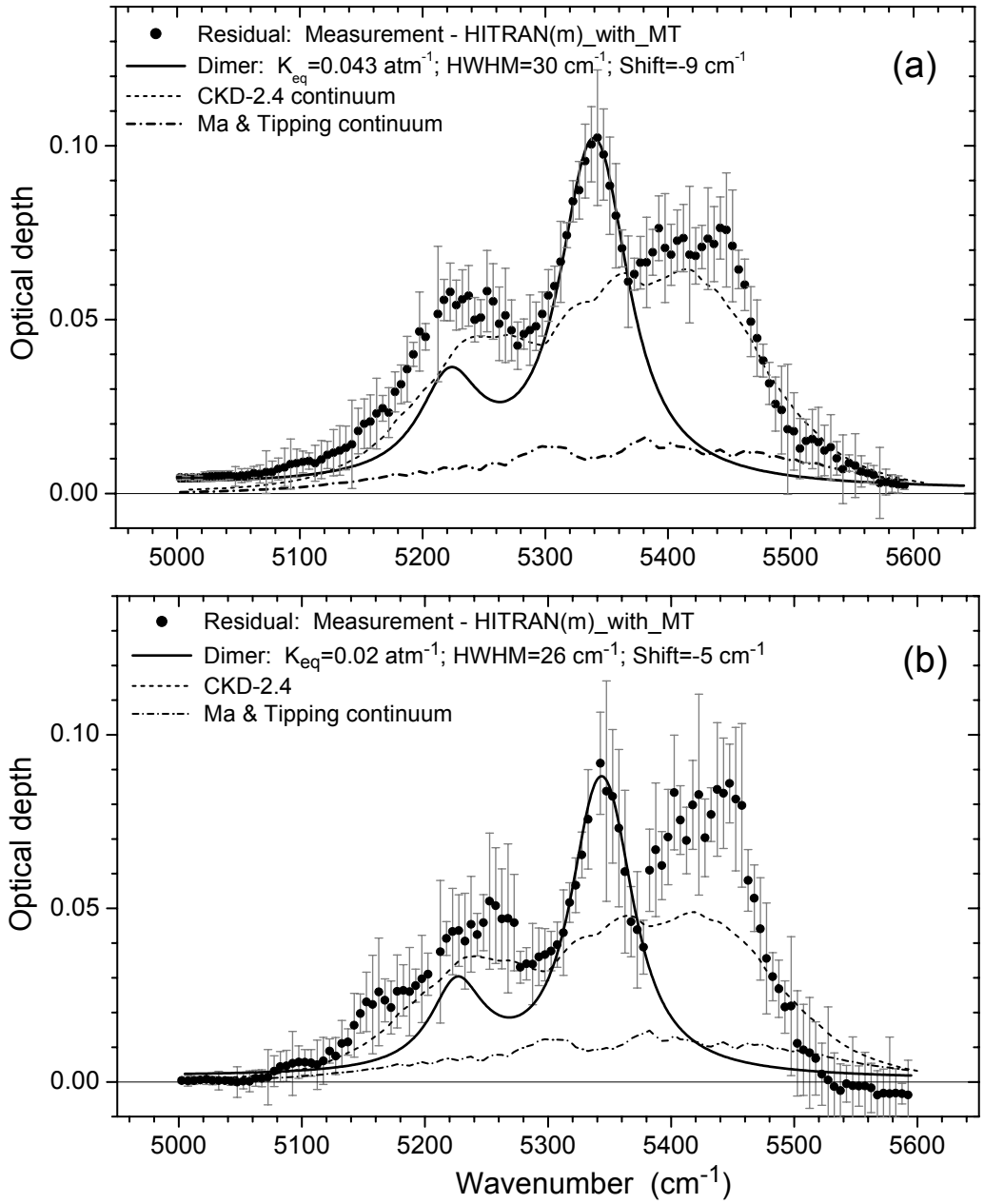
Residual: Measurement - HITRAN(m)_with_MT
Dimer: K_{eq}=0.043 atm^{-1}; HWHM=30 cm^{-1}; Shift=-9 cm^{-1}
CKD-2.4 continuum
Ma & Tipping continuum
(a)
Optical depth
0.00
0.05
0.10
5000
5100
5200
5300
5400
5500
5600
Residual: Measurement - HITRAN(m)_with_MT
Dimer: K_{eq}=0.02 atm^{-1}; HWHM=26 cm^{-1}; Shift=-5 cm^{-1}
CKD-2.4
Ma & Tipping continuum
(b)
Optical depth
0.00
0.05
0.10
5000
5100
5200
5300
5400
5500
5600
Wavenumber (cm^{-1})

Figure 5.

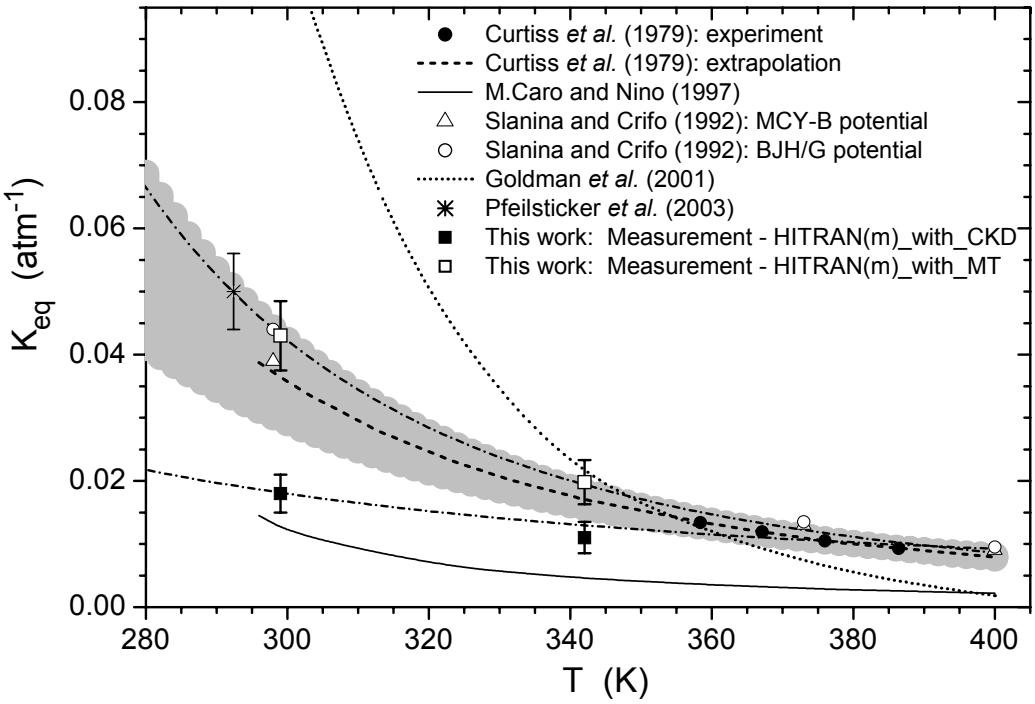

Figure 6.

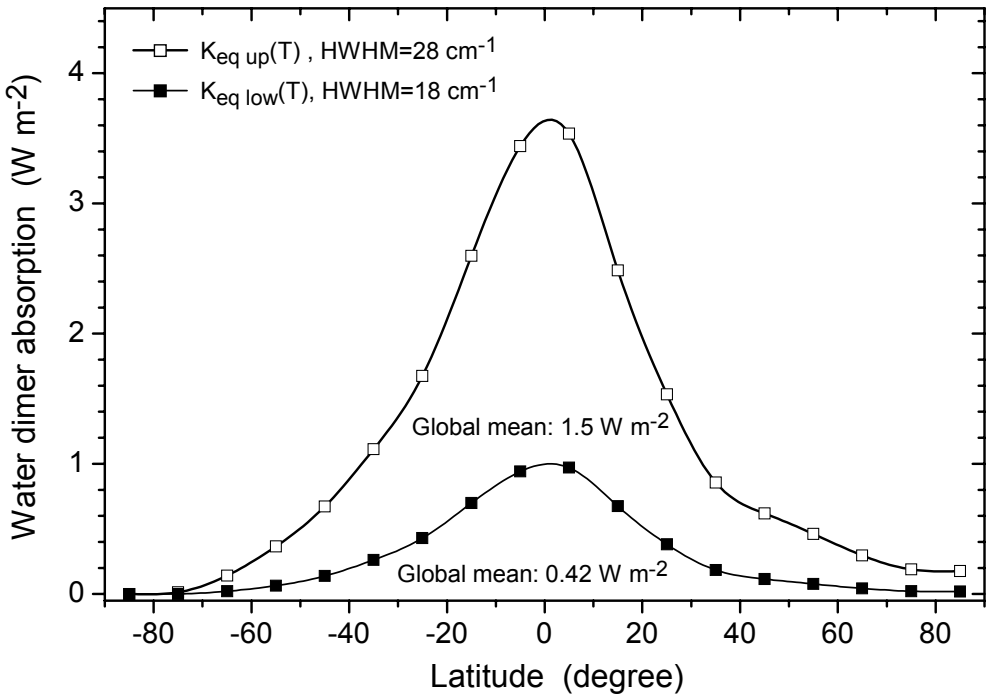

Figure 7.

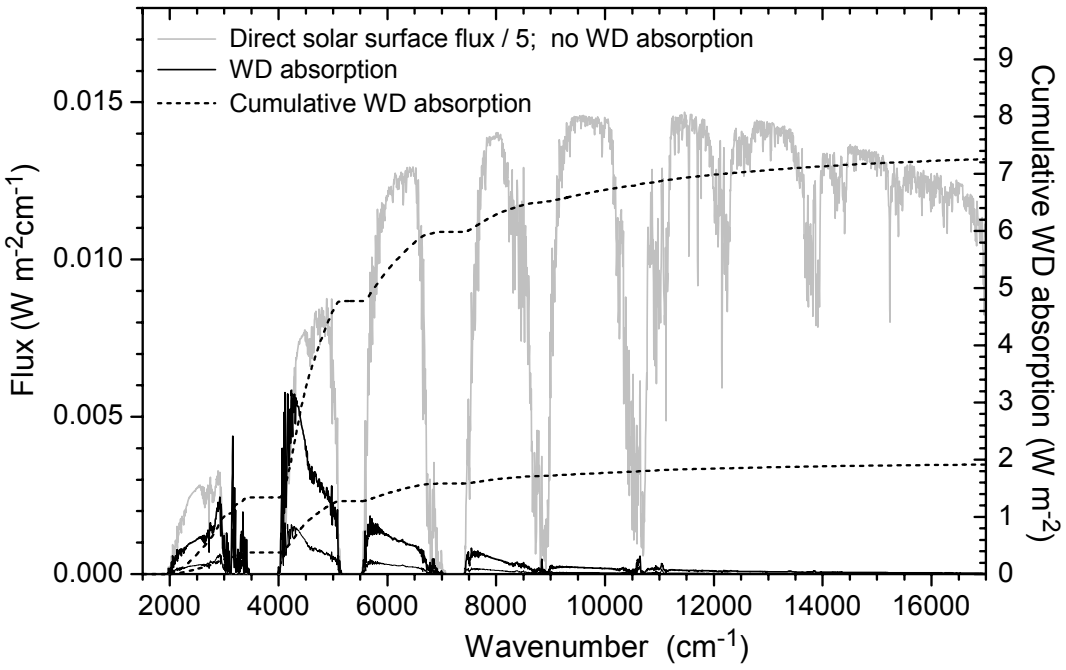

Figure 8.

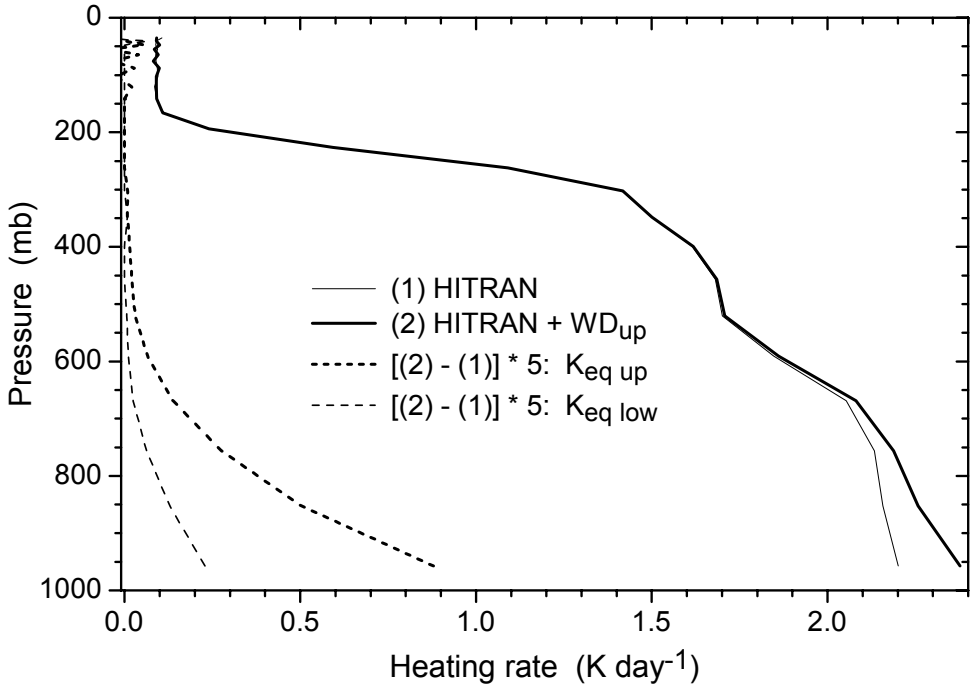

Figure 9.